Highly Birefringent Terahertz Metasurfaces Based on a Liquid-Crystal-Embedded Metal Mesh

Tomoyuki Sasaki ⬤, Mami Harada ⬤, Moritsugu Sakamoto, Kohei Noda, Keiichi Itoh ⬤, Hiroyuki Okamoto, and Hiroshi Ono

Abstract—Here, we report a metasurface for polarization converters in the terahertz (THz) spectral range. The THz metasurface consists of a metal mesh with subwavelength isotropic apertures and a nematic liquid crystal (LC) that is a uniaxially anisotropic dielectric medium. The LC is embedded and aligned homogeneously in the apertures. We calculated the complex transmittance and complex reflectance of the LC-embedded metal mesh (LC metasurface) for the eigen-polarization states using the finite-difference time-domain method, and we then investigated the effective electromagnetic parameters. The LC metasurface exhibits birefringence of approximately 1, which is one order of magnitude larger than that of the LC, in the transmission band. We also investigated the relationship between the geometrical parameters of the LC metasurface and transmissive retardation. These results demonstrate that the LC metasurface is useful for transmissive polarization converters in the THz spectral range.

Index Terms—Metamaterial, metasurface, liquid crystal, terahertz device.

I. INTRODUCTION

ELECTROMAGNETIC metamaterials, including liquid crystals (LCs), are of interest in a wide frequency range because of their tunability with external fields [1]–[15]. In particular, the practical value of the LC-containing metamaterials (LC metamaterials) is extremely high in the terahertz (THz) spectral range owing to the lack of media for active THz devices. Shekenhamer *et al.* presented an experimental demonstration of LC metamaterials for electrically tunable THz absorbers [6]. Buchnev *et al.* reported intensity and phase modulation of THz radiation using an actively controlled large-area LC

Tomoyuki Sasaki, Mami Harada, Moritsugu Sakamoto, Kohei Noda, and Hiroshi Ono are with the Department of Electrical Engineering, Nagaoka University of Technology, Nagaoka, Niigata 940-2188, Japan (e-mail: sasaki_tomoy@vos.nagaokaut.ac.jp; s171069@stn.nagaokaut.ac.jp; sakamoto@vos. nagaokaut.ac.jp; noda@konomi.nagaokaut.ac.jp; onoh@vos.nagaokaut.ac.jp).

Keiichi Itoh is with the School of Creative System Engineering, National Institute of Technology, Akita College, Akita 011-8511, Japan (e-mail: itok@akita-nct.ac.jp).

Hiroyuki Okamoto is with the Department of Creative Technology Engineering, National Institute of Technology, Anan College, Anan, Tokushima 774-0017, Japan (e-mail: okamoto@anan-nct.ac.jp).

metamaterial [7]. Wu *et al.* proposed a cording LC metasurface to manipulate the THz beam dynamically [14]. These studies demonstrate the usefulness of LC metamaterials for various active THz devices.

LCs without metallic subwavelength structures can also realize fundamental active THz elements, such as phase, polarization, and intensity modulators [16]–[22]. However, these LC THz elements have a problem in the response speeds [20], [21]. To obtain a sufficient phase shift or retardation for THz waves, the thickness of the LC layer should be comparable with the submillimeter to millimeter wavelength [15], [19]. For example, in planarly aligned nematic LCs, which are dielectric media with uniaxial anisotropy, the alignment transition time for the applied electric field is proportional to the square of the thickness of the LC layer [23]. Therefore, the response speeds of common LC THz elements are much lower than those of LC elements in the visible range. LC metamaterials also have the potential to improve this problem. Zografopoulos and Beccherelli theoretically investigated the electrical tunable properties of THz LC metamaterials consisting of metal–LC–metal cavity structures for fast switching [10]. They reported that the calculated response speed of the THz LC metamaterial is orders of magnitude faster than that in the LC-based non-resonant THz components [10]. Vasić *et al.* reported that metal–LC–metal metamaterials allow the THz polarization converter to operate at driving voltages below 10 V with millisecond switching times [11].

Recently, we proposed a THz metasurface consisting of a nematic LC and a subwavelength metal mesh [24]. Metal meshes with subwavelength apertures exhibit extraordinary transmission, and they have been used as frequency selective surfaces (FSSs), such as THz bandpass filters [25]–[27]. The extraordinary transmission in the THz spectral range is generally explained by a coupled-mode model of spoof surface plasmon polaritons [28]. In our previous study, based on experiments and numerical simulations, we demonstrated that the LC metasurface converts the polarization state of the THz wave in the transmission process and the thickness of the LC layer can be reduced by two orders of magnitude relative to the planarly aligned LC without metal meshes [24]. As mentioned above, this is an advantage for the response speed in active control. However, the electromagnetic properties of the LC metasurface have not been quantitatively studied, and the design concepts for practical applications have not been obtained.

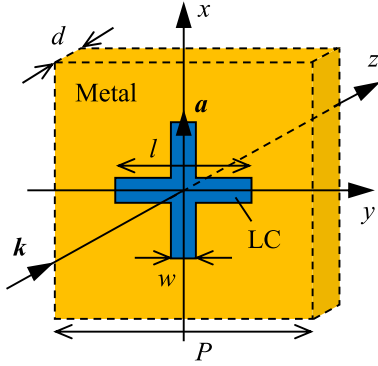In the present study, to obtain insight into the mechanism of the polarization conversion, we investigated the electromagnetic

Fig. 1.   Schematic of the unit cell of the LC metasurface. **a** is the alignment direction of the nematic LC. **k** is the wave vector of the incident wave.

properties of THz LC metasurfaces consisting of a metal mesh with subwavelength isotropic apertures and a nematic LCs. The complex transmittance and complex reflectance of the LC metasurface were simulated for the eigen-polarization states by the finite-difference time-domain (FDTD) method. Based on the simulation results, we characterized the effective electromagnetic parameters and investigated the relationship between the retardation of the eigen-polarization states and the geometrical parameters of the aperture. This study provides the basic design concept of LC metasurfaces for THz polarization converters.

II. CALCULATION METHODS

In this study, we considered a LC metasurface consisting of a free-standing isotropic metal mesh with subwavelength cross apertures. These metal meshes are expected to be FSSs in the THz spectral range [25]–[27]. The unit cell of the LC metasurface is shown in Fig. 1. We assumed that a nematic LC was uniaxially aligned in the apertures, as shown in Fig. 1. The two arms of the cross aperture were parallel to the x- or y-direction. For the cross aperture, the lengths and widths of the arms were the same for the x- and y-directions. The unit cell size for the x- and y-directions was set to be $P = 270$ μm for future experimental demonstration [24]. The arm length l, arm width w, and thickness of the metal mesh (i.e., the thickness of the LC layer) d were variables. The metal was assumed to be a perfect electric conductor (PEC), and the nematic LC was assumed to be a lossless dielectric material with positive uniaxial anisotropy. The LC was aligned in the x-direction in the apertures. The ordinary and extraordinary refractive indices of the LC were set to be $n_o = 1.54$ and $n_e = 1.69$, respectively, which are the values of 4-penthyl-4′-cyanobiphenyl (5CB), which is a common nematic LC, in the THz spectral range [29]. The birefringence of the LC was $\Delta n = n_e - n_o = 0.15$. Because the metal mesh was isotropic and the LC was aligned to the x-axis, the eigen-polarization states of the metasurface were linear polarization parallel to the x- and y-directions. We calculated the complex transmittance and complex reflectance of the LC metasurface at normal incidence for the eigen-polarization states using a FDTD simulator (Ansys Lumerical FDTD). In the FDTD simulation, we assumed that the free space surrounding the LC metasurface was a vacuum (i.e., the refractive index of

the free space was 1). The sampling points of the transmitted and reflected waves in the free space were sufficiently far from the LC metasurface. As boundary conditions, perfectly matched layers were introduced in the z-direction and periodic boundary conditions were introduced in the x- and y-directions. Actually, we will use the metal mesh sandwiched between dielectric substrates with alignment layers as shown in [24], instead of the free-standing metal mesh. However, since the LC apertures are essentially important in the polarization conversion property, we employ the free-standing metal mesh without substrates in this study.

Based on the results of the FDTD simulation, we characterized the effective electromagnetic parameters of the LC metasurface. The effective wave impedance for the eigen-polarization states can be expressed as

$$Z_q = \pm Z_f \sqrt{\frac{(1 + r_q)^2 - t_q^2}{(1 - r_q)^2 - t_q^2}}, \qquad (1)$$

where q is x or y (i.e., Z_q is the effective wave impedance for the linearly polarized wave parallel to the q-direction), Z_f is the wave impedance of the free space, t_q is the complex transmittance for the linearly polarized wave parallel to the q-direction, and r_q is the complex reflectance for the linearly polarized wave parallel to the q-direction [30]–[32]. The double-sign in (1) can be selected based on $\text{Re} Z_q \geq 0$ because the material has no gain. The effective complex refractive index for the eigen-polarization states $\hat{n}_q$ is given by

$$\cos(k_0 \hat{n}_q d) = \frac{1 - r_q^2 + t_q^2}{2 t_q} \equiv G_q, \qquad (2)$$

where k_0 is the wavenumber of the incident wave in vacuum [30]–[32]. Because $\hat{n}_q$ is a complex number, the effective refractive index $\text{Re} \hat{n}_q \equiv n_q$ and the effective extinction coefficient $\text{Im} \hat{n}_q \equiv \kappa_q$ are expressed as

$$n_q = \frac{1}{k_0 d} \text{Im} \left[\ln \left(G_q \pm \sqrt{1 - G_q^2} \right) \right], \qquad (3)$$

$$\kappa_q = -\frac{1}{k_0 d} \text{Re} \left[\ln \left(G_q \pm \sqrt{1 - G_q^2} \right) \right], \qquad (4)$$

where the double-sign in (3) corresponds to that in (4). A unique value for κ_q can be obtained because $\kappa_q \geq 0$ and $\text{Re}(\ln A)$ is a single-valued function, where A is a complex number. However, n_q is not uniquely determined because $\text{Im}(\ln A)$ has infinite branches. Here, (3) is rewritten as

$$n_q = N_q + \frac{2\pi m}{k_0 d}, \qquad (5)$$

where N_q is the principal value of n_q determined by the principal branch in (3) and m is an integer. In this study, we defined the effective birefringence as $\Delta N = N_x - N_y$ and the effective retardation as $\gamma = k_0 \Delta N d$, where $-\pi < \gamma \leq \pi$.

III. RESULTS AND DISCUSSION

The frequency spectra of the zeroth order transmittance $|t_q|^2 \equiv T_q$ and the phase $\arg t_q$ for $d = 40$ μm , $w = 20$ μm,
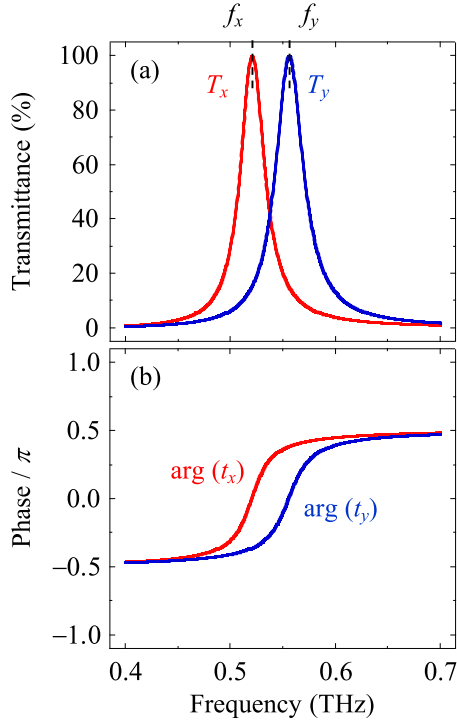
Fig. 2. Transmittance and phase for $d = 40\ \mu$m, $w = 20\ \mu$m, and $l = 170\ \mu$m. (a) Transmittance. (b) Phase in units of π.

Fig. 3. Effective electromagnetic parameters for $d = 40\ \mu$m, $w = 20\ \mu$m, and $l = 170\ \mu$m. (a) Wave impedance normalized by $Z_{\rm f}$. (b) Complex refractive index. (c) Birefringence.

and $l = 170\ \mu$m are shown in Fig. 2. The LC metasurface can also be used as a bandpass filter in the THz spectral range [Fig. 2(a)]. However, the transmission frequency depends on the polarization state of the incident wave. Here, as shown in Fig. 2(a), we define the frequency as f and the peak frequency with the maximal transmittance for the linear polarization parallel to the q-axis as f_q. Because $T_q(f_q) = 1$, it was surmised that the wave impedances of the LC metasurface and free space are effectively matched at $f = f_q$. The phase is not proportional to the frequency and show a rapid change around f_q [Fig. 2(b)]. This indicates that the phase difference between the eigen-polarization states can be controlled by the refractive indices of the LC and/or the alignment direction of the LC. Additionally, we show the transmittance and phase spectra of an isotropic-dielectric-embedded metal mesh in Fig. S1.

The frequency spectra of the effective parameters for $d = 40\ \mu$m , $w = 20\ \mu$m, and $l = 170\ \mu$m are shown in Fig. 3. Here, we have confirmed that the transmittance and phase spectra shown in Fig. 2 are reproduced using the effective parameters shown in Fig. 3 and the Fresnel equations. Z_q and $\hat{n}_q$ exhibit drastic changes around f_q [Fig. 3(a) and 3(b)]. For both eigen-polarization states, $Z_q(f < f_q)$ is inductive while $Z_q(f > f_q)$ is almost purely resistive. In addition, $\kappa_q(f > f_q) \simeq 0$ and $N_q(f < f_q) \simeq 0$. At $f = f_q$, the impedance matching to the free space (i.e., $Z_q/Z_{\rm f} \simeq 1$) is achieved. As shown in Fig. 3(c), ΔN also shows strong frequency dispersion. We define the peak frequency with the maximal effective birefringence as f_γ [Fig. 3(c)]. In this case, $\Delta N(f_\gamma) \simeq 0.90$. This value is 6 times
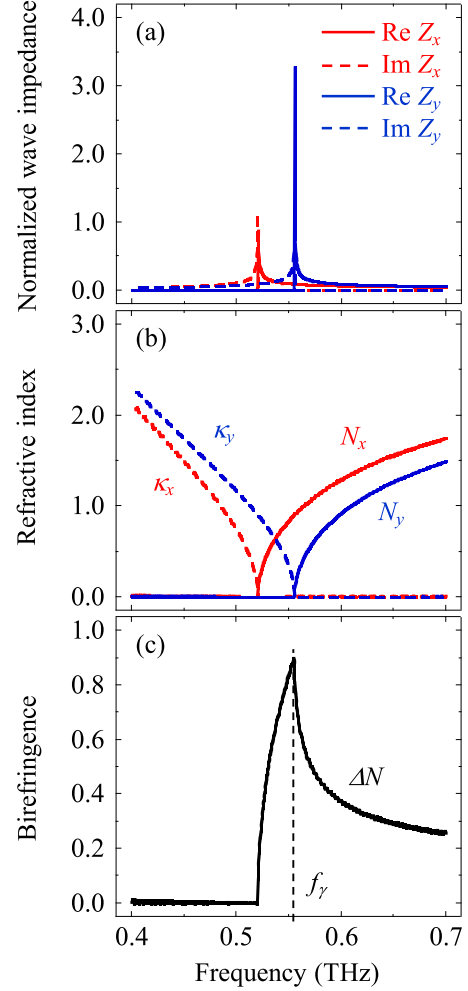
higher than Δn. Namely, enhancement of the birefringence can be realized using the isotropic metal mesh.

For practical applications of the LC metasurface, the phase difference between the eigen-polarization states (i.e., the retardation) is more important than the effective birefringence. The above defined effective retardation γ, which is formally proportional to ΔN and d, is caused by propagation in the medium. However, the phase also changes due to the difference between the impedances of the free space and medium. This is because the Fresnel coefficients between the boundaries (i.e., the argument of the complex transmittance) depend on Z_q, which is a complex number. Here, we characterize the integrated retardation considering both the propagation and boundaries. Using the argument of t_q, the integrated retardation in the transmission process is defined as

$$\Gamma = \arg t_x - \arg t_y, \qquad (6)$$

where $-\pi < \Gamma \leq \pi$. The frequency spectra of γ and Γ for $d = 40\ \mu$m, $w = 20\ \mu$m, and $l = 170\ \mu$m are shown in Fig. 4. The peak frequency with the maximal Γ is denoted f_Γ. In this case,
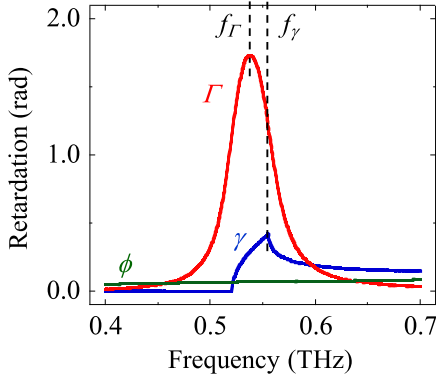
Fig. 4. Retardation for $d = 40\ \mu$m, $w = 20\ \mu$m, and $l = 170\ \mu$m.

$f_\Gamma \simeq 0.538$ THz $\neq f_\gamma$. For common isotropic metal meshes, the phase changes rapidly around the peak frequency of the transmittance [28]. Therefore, a large integrated retardation can be obtained by controlling f_q that depends on the geometrical parameters and the refractive indices in the apertures. Using the peak wavelength $\lambda_\Gamma = c_0/f_\Gamma \simeq 558\ \mu$m, the geometrical parameters are normalized as $P/\lambda_\Gamma \simeq 0.484$, $d/\lambda_\Gamma \simeq 0.072$, $w/\lambda_\Gamma \simeq 0.036$, and $l/\lambda_\Gamma \simeq 0.305$, where c_0 is the speed of light in vacuum. For these geometrical parameters, we obtained $\Gamma(f_\Gamma) \simeq 1.73$ rad. This value is higher than $\gamma(f_\gamma)$ and the retardation of the homogeneous LC layer $\phi = k_0\Delta n d$ at $f = f_\Gamma$ (Fig. 4). Namely, retardation can be achieved with $> \pi/2$ in the transmission process by adjusting the geometrical parameters of the aperture. This indicates that the LC metasurface is useful for transmissive polarization converters and phase shifters in the THz spectral range.

To obtain insight into the maximization of $\Gamma(f_\Gamma)$, we investigated the relationship between the geometrical parameters (i.e., d, w, and l) and $\Gamma(f_\Gamma)$ based on the FDTD simulation. The results are summarized in Figs. 5–7. The thickness dependence for $w = 20\ \mu$m and $l = 170\ \mu$m is shown in Fig. 5. $\Gamma(f_\Gamma)$ increases with increasing d. However, $\Gamma(f_\Gamma)$ is not proportional to d, unlike ϕ, and $\partial\Gamma(f_\Gamma)/\partial d$ decreases with increasing d [Fig. 5(a)]. The thickness also affects f_Γ because the peak frequencies of T_q and $\arg t_q$ are shifted continuously by varying d [28]. In contrast to $\Gamma(f_\Gamma)$, $T_x(f_\Gamma)$ and $T_y(f_\Gamma)$ decrease with increasing d [Fig. 5(b)]. Namely, there is a trade-off between the integrated retardation and the transmittance. Here, at $f = f_\Gamma$, we define the transmittance ratio as

$$\rho = \begin{cases} T_x/T_y & \text{for } T_x \leq T_y \\ T_y/T_x & \text{for } T_x > T_y \end{cases}, \tag{7}$$

where $0 \leq \rho \leq 1$. In the case of $\rho = 1$, the transmittances for the eigen-polarization states are the same. To control the phase and/or polarization states purely, it is desirable that ρ is close to 1. As shown in Fig. 5(b), $\rho \simeq 1$ can be obtained by controlling the geometrical parameters. This is an advantage of the LC metasurface for practical applications. When the absolute values of the x- and y-components of the electric field of the incident wave are equal, the Jones vector of the incident wave is written as $\mathbf{E}_{in} = A[1\ \exp(i\delta)]$, where A is the amplitude and δ is the initial phase difference between the y- and x-components. For $f = f_\Gamma$
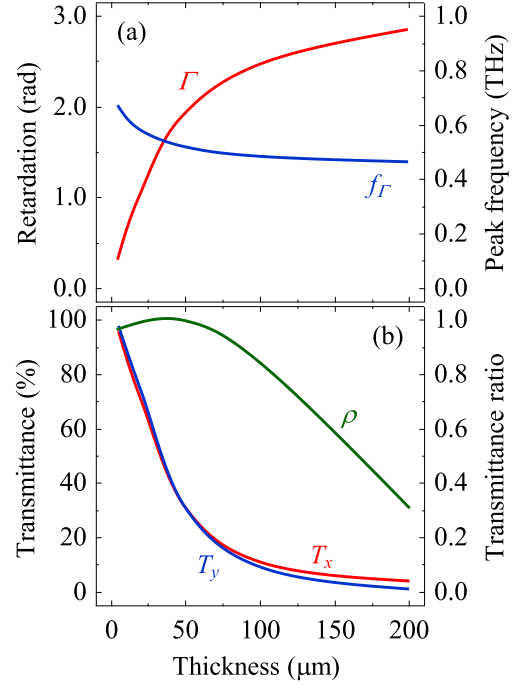

Fig. 5. Thickness dependence for $w = 20\ \mu$m and $l = 170\ \mu$m. (a) Integrated retardation $\Gamma(f_\Gamma)$ and peak frequency f_Γ. (b) Transmittance T_x and T_y and transmittance ratio ρ.

Fig. 6. Width dependence for $d = 10\ \mu$m and $l = 170\ \mu$m. (a) Integrated retardation $\Gamma(f_\Gamma)$ and peak frequency f_Γ. (b) Transmittance T_x and T_y and transmittance ratio ρ.
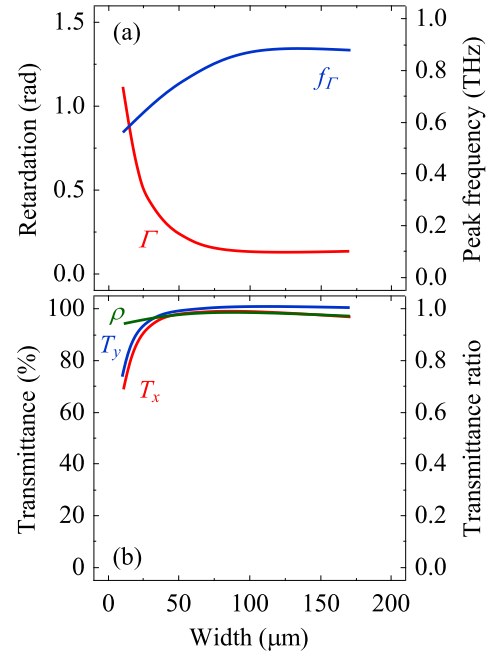
and $\rho = 1$, the Jones vector of the transmitted wave is written as $\mathbf{E}_{out} = \sqrt{T}A[1\ \exp[i(\delta - \Gamma)]]$, where $T = T_x = T_y$. Namely, the polarization state of the transmitted wave can be controlled by Γ without changing the intensity. The line-width dependence for $d = 10\ \mu$m and $l = 170\ \mu$m is shown in Fig. 6. $\Gamma(f_\Gamma)$ can be increased by decreasing w [Fig. 6(a)], but $T_x(f_\Gamma)$ and $T_y(f_\Gamma)$
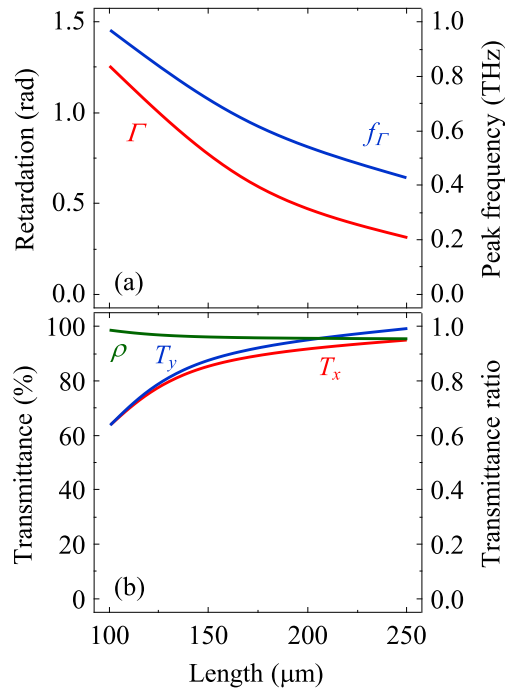
Fig. 7. Length dependence for $d = 10$ μm and $w = 20$ μm. (a) Integrated retardation $\Gamma(f_\Gamma)$ and peak frequency f_Γ. (b) Transmittance T_x and T_y and transmittance ratio ρ.

decrease by decreasing w [Fig. 6(b)]. The line-length dependence for $d = 10$ μm and $w = 20$ μm is shown in Fig. 7. The results shown in Figs. 6 and 7 indicate that the integrated retardation increases with decreasing aperture size. However, there is also a trade-off relationship between the integrated retardation and the transmittance. Namely, the LC metasurface is useful for transmissive THz modulators, but optimization of the unit cell structure is important for practical applications. We are currently studying optimization of the aperture form and the geometrical parameters based on the machine learning approach.

Additionally, same simulation results are shown in Figs. S2–S4. These data are useful for understanding effects of substrates and losses in the metal and LC. In particular, the additional data indicates that it is important to use a LC with small extinction coefficients in practical applications.

IV. CONCLUSION

We have numerically simulated the electromagnetic properties of a THz metasurface consisting of a uniaxially anisotropic LC and a subwavelength metal mesh with isotropic apertures. Based on the complex transmittance/reflectance, the wave impedance, refractive index, and birefringence were formally characterized. As a result, we demonstrated that the LC metasurface exhibits birefringence that is several times higher than that of the LC embedded in the apertures. The integrated retardation between the eigen-polarization states was also characterized by considering the phase changes both at the boundaries and in the LC metasurface. We found that the LC metasurface can realize high retardation with $> \pi/2$ for proper geometrical parameters in the transmission process. At this point, we cannot

sufficiently explain the physical meaning of the obtained results. However, we believe that our simulation results are important for demonstrating the usefulness of the LC-embedded metal meshes as media for THz polarization convertors and modulators. We would like to discuss the construction of analytical models and the qualitative explanation of the properties in further work.

REFERENCES

[1] Q. Zhao *et al.*, "Electrically tunable negative permeability metamaterials based on nematic liquid crystals," *Appl. Phys. Lett.*, vol. 90, no. 1, 2007, Art. no. 011112.
[2] M. V. Gorkunov and M. A. Osipov, "Tunability of wire-grid metamaterial immersed into nematic liquid crystal," *J. Appl. Phys.*, vol. 103, no. 3, 2008, Art. no. 036101.
[3] I. C. Khoo, A. Diaz, L. Liou, M. V. Stinger, J. Huang, and T. Ma, "Liquid crystals tunable optical metamaterials," *IEEE J. Sel. Topics Quantum Electron.*, vol. 16, no. 2, pp. 410–417, Mar./Apr. 2010.
[4] A. Minovich *et al.*, "Liquid crystal based nonlinear fishnet metamaterials," *Appl. Phys. Lett.*, vol. 100, no. 12, 2012, Art. no. 121113.
[5] M. Decker *et al.*, "Electro-optical switching by liquid-crystal controlled metasurfaces," *Opt. Exp.*, vol. 21, no. 7, pp. 8879–8885, 2013.
[6] D. Shrekenhamer, W.-C. Chen, and W. J. Padilla, "Liquid crystal tunable metamaterial absorber," *Phys. Rev. Lett.*, vol. 110, no. 15, 2013, Art. no. 151903.
[7] O. Buchnev, J. Wallauer, M. Walther, M. Kaczmarek, N. I. Zheludev, and V. A. Fedotov, "Controlling intensity and phase of terahertz radiation with an optically thin liquid crystal-loaded metamaterial," *Appl. Phys. Lett.*, vol. 130, no. 14, 2013, Art. no. 141904.
[8] R. Kowerdziej, M. Oilferczuk, J. Parka, and J. Wróbel, "Terahertz characterization of tunable metamaterial based on electrically controlled nematic liquid crystal," *Appl. Phys. Lett.*, vol. 150, no. 2, 2014, Art. no. 022908.
[9] G. Isić, B. Vasić, D. C. Zografopoulos, R. Beccherelli, and R. Gajić, "Electrically tunable critically coupled terahertz metamaterial absorber based on nematic liquid crystals," *Phys. Rev. Appl.*, vol. 3, no. 6, 2015, Art. no. 064007.
[10] D. C. Zografopoulos and R. Beccherelli, "Terahertz fishnet metamaterials based on thin nematic liquid crystal layers for fast switching," *Sci. Rep.*, vol. 5, 2015, Art. no. 13137.
[11] B. Vasić, D. C. Zografopoulos, G. Isić, R. Beccherelli, and R. Gajić, "Electrically tunable terahertz polarization converter based on overcoupled metal-isolator-metal metamaterials infiltrated with liquid crystals," *Nanotechnology*, vol. 28, no. 12, 2017, Art. no. 124002.
[12] T. Sasaki *et al.*, "Liquid crystal cells with subwavelength metallic gratings for transmissive terahertz elements with electrically tunability," *Opt. Commun.*, vol. 431, pp. 63–67, 2019.
[13] S.-T. Xu, F. Fan, Y.-Y. Ji, J.-R. Cheng, and S.-J. Chang, "Terahertz resonance switch induced by the polarization conversion of liquid crystal in compound metasurface," *Opt. Lett.*, vol. 44, no. 10, pp. 2450–2453, 2019.
[14] J. Wu *et al.*, "Liquid crystal programmable metasurface for terahertz beam steering," *Appl. Phys. Lett.*, vol. 116, no. 13, 2020, Art. no. 131104.
[15] J. Xu, R. Yang. Y. Fan, Q. Fu, and F. Zhang, "A review of tunable electromagnetic metamaterials with anisotropic liquid crystals," *Front. Phys.*, vol. 9, 2021, Art. no. 633104.
[16] H.-Y. Wu, C.-F. Hsieh, T.-T. Tang, R.-P. Pan, and C.-L. Pan, "Electrically tunable room-temperature 2π liquid crystal terahertz phase shifter," *IEEE Photon. Technol. Lett.*, vol. 18, no. 14, pp. 1488–1490, Jul. 2006.
[17] T. Sasaki, K. Noda, N. Kawatsuki, and H. Ono, "Universal polarization terahertz phase controllers using randomly aligned liquid crystal cells with graphene electrodes," *Opt. Lett.*, vol. 40, no. 7, pp. 1544–1547, 2015.
[18] C. Yang, C. Kuo, C. Tang, J. C. Chen, R. Pan, and C. Pan, "Liquid-crystal terahertz quarter-wave plate using chemical-vapor-deposited graphene electrodes," *IEEE Photon. J.*, vol. 7, no. 6, Dec. 2015, Art. no. 2200808.

[19] X. Li, N. Tan, M. Pivnenko, J. Sibil, J. A. Zeitler, and D. Chu, "High-birefringence nematic liquid crystal for broadband THz applications," *Liquid Crystals*, vol. 43, no. 7, pp. 955–962, 2016.

[20] T. Sasaki *et al.*, "Twisted nematic liquid crystal cells with rubbed poly(3,4-ethylenedioxythiophene)/poly(styrenesulfonate) films for active polarization control of terahertz wave," *J. Appl. Phys.*, vol. 121, no. 14, 2017, Art. no. 143106.

[21] T. Sasaki, H. Okuyama, M. Sakamoto, K. Noda, N. Kawatsuki, and H. Ono, "Optical control of polarized terahertz waves using dye-doped nematic liquid crystals," *AIP Adv.,* vol. 8, no. 11, 2018, Art. no. 115326.

[22] T. Sasaki *et al.*, "Subwavelength liquid crystal gratings for polarization-independent phase shifts in the terahertz spectral range," *Opt. Mater. Exp.*, vol. 10, no. 2, pp. 240–248, 2020.

[23] P. Yeh and G. Gu, *Optics of Liquid Crystal Displays*. Hoboken, NJ, USA: Wiley, 1997.

[24] T. Sasaki *et al.*, "Active terahertz polarization conversion using a liquid crystal-embedded metal mesh," *IEEE Photon. J.*, vol. 11, no. 6, Dec. 2019, Art. no. 5901007.

[25] M. E. MacDonald, A. Alexanian, R. A. York, Z. Popović, and E. N. Grossman, "Spectral transmittance of lossy printed resonant-grid terahertz bandpass filters," *IEEE Trans. Microw. Theory Technol.*, vol. 48, no. 4, pp. 712–718, Apr. 2000.

[26] A. M. Melo *et al.*, "Metal mesh resonant filters for terahertz frequencies," *Appl. Opt.*, vol. 47, no. 32, pp. 6064–6069, 2008.

[27] A. Ferraro, D. C. Zografopoulos, R. Caputo, and R. Beccherelli, "Broad- and narrow-line terahertz filtering in frequency-selective surfaces patterned on thin low-loss polymer substrates," *IEEE J. Sel. Topics Quantum Electron.*, vol. 23, no. 4, Jul./Aug. 2017, Art. no. 8501308.

[28] F. J. Garcia-Vidal, L. Martin-Moreno, T. W. Ebbesem, and L. Kuipers, "Light passing through subwavelength apertures," *Rev. Modern Phys.*, vol. 82, no. 59, pp. 729–787, 2010.

[29] N. Vieweg, M. K. Shakfa, B. Scherger, M. Mikulics, and M. Koch, "THz properties of nematic liquid crystals," *J. Infrared Millimeter Terahertz Waves*, vol. 31, no. 11, pp. 1313–1320, 2010.

[30] D. R. Smith, S. Schultz, P. Markoš, and C. M. Souloulis, "Determination of effective permittivity and permeability of metamaterials from reflection and transmission coefficients," *Phys. Rev. B*, vol. 65, no. 19, 2002, Art. no. 195104.

[31] X. Chen, T. M. Grezegorczyk, B.-I. Wu, J. Pacheco, Jr., and J. A. Kong, "Robust method to retrieve the constitutive effective parameters of metamaterials," *Phys. Rev. E*, vol. 70, no. 1, 2004, Art. no. 016608.

[32] D. R. Smith, D. C. Vier, Th. Koschny, and C. M. Soukoulis, "Electromagnetic parameter retrieval from inhomogeneous metamaterials," *Phys. Rev. E*, vol. 71, no. 3, 2005, Art. no. 036617.